BIOCHEMISTRY
including biophysical chemistry & molecular biology

Article

pubs.acs.org/biochemistry

Structure, Dynamics, and Antimicrobial and Immune Modulatory Activities of Human LL-23 and Its Single-Residue Variants Mutated on the Basis of Homologous Primate Cathelicidins

Guangshun Wang,*[,†] Melissa Elliott,[‡] Anna L. Cogen,[§] Edward L. Ezell,[∥] Richard L. Gallo,[§] and Robert E. W. Hancock[‡]

[†]Department of Pathology and Microbiology, College of Medicine, University of Nebraska Medical Center, 986495 Nebraska Medical Center, Omaha, Nebraska 68198-6495, United States

[‡]Department of Microbiology and Immunology, University of British Columbia, Room 232, 2259 Lower Mall Research Station, Vancouver, British Columbia, Canada V6T 1Z4

[§]Division of Dermatology, Department of Medicine, University of California at San Diego, 9350 Campus Point Drive, La Jolla, California 92037, United States

[∥]Eppley Institute for Research in Cancer and Allied Diseases, University of Nebraska Medical Center, Omaha, Nebraska 68198-6805, United States

ABSTRACT: LL-23 is a natural peptide corresponding to the 23 N-terminal amino acid residues of human host defense cathelicidin LL-37. LL-23 demonstrated, compared to LL-37, a conserved ability to induce the chemokine MCP-1 in human peripheral blood mononuclear cells, a lack of ability to suppress induction of the pro-inflammatory cytokine TNF-α in response to bacterial lipopolysaccharides (LPS), and reduced antimicrobial activity. Heteronuclear multidimensional nuclear magnetic resonance (NMR) characterization of LL-23 revealed similar secondary structures and backbone dynamics in three membrane-mimetic micelles: SDS, dodecylphosphocholine (DPC), and dioctanoylphosphatidylglycerol. The NMR structure of LL-23 determined in perdeuterated DPC contained a unique serine that segregated the hydrophobic surface of the amphipathic helix into two domains. To improve our understanding, Ser9 of LL-23 was changed to either Ala or Val on the basis of homologous primate cathelicidins. These changes made the hydrophobic surface of LL-23 continuous and enhanced antibacterial activity. While identical helical structures did not explain the altered activities, a reduced rate of hydrogen−deuterium exchange from LL-23 to LL-23A9 to LL-23V9 suggested a deeper penetration of LL-23V9 into the interior of the micelles, which correlated with enhanced activities. Moreover, these LL-23 variants had discrete immunomodulatory activities. Both restored the TNF-α dampening activity to the level of LL-37. Furthermore, LL-23A9, like LL-23, maintained superior protective MCP-1 production, while LL-23V9 was strongly immunosuppressive, preventing baseline MCP-1 induction and substantially reducing LPS-stimulated MCP-1 production. Thus, these LL-23 variants, designed on the basis of a structural hot spot, are promising immune modulators that are easier to synthesize and less toxic to mammalian cells than the parent peptide LL-37.

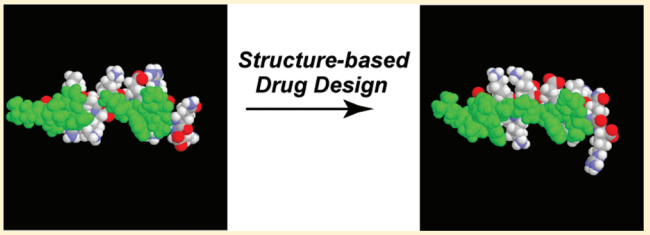

Naturally occurring antimicrobial peptides (AMPs) are key components of the innate immune systems of all life forms.[1−6] The current version of the antimicrobial peptide database (http://aps.unmc.edu/AP/main.html/) contained 1800 AMPs as of October 2011. Among them, 151 entries originated from bacteria, 250 from plants, and 1283 from animals.[7,8] In the case of animal AMPs, 665 were discovered from amphibians, primarily frog skin. Likewise, AMPs such as LL-37, β-defensins, dermcidin, psoriasin (S100A7), and RNase 7 were detected in human skin,[9,10] and some of them can be produced upon UV irradiation.[11] LL-37 exists in infant skin, as well.[12] The protective role of human host defense cathelicidin LL-37 against infection has been demonstrated in animal models.[13,14] In human skin, the activity of LL-37 is regulated by proteases at two levels: generation from its precursor protein hCAP-18 and degradation to smaller fragments, which may, or may not, be biologically active. Several active fragments of LL-37 have been detected in healthy human skin, including LL-23, LL-29, and KS-27.[15] The protease that cleaves hCAP-18 into LL-37 in neutrophils is proteinase 3, while other proteases such as kallikreins are proposed to cut LL-37 into smaller fragments in the skin. Importantly, the peptide cleavage pattern in healthy skin differs from that of diseased skin, suggesting that AMP profiles have potential diagnostic value and/or functional importance.[16]

Received: October 25, 2011
Revised: December 7, 2011
Published: December 20, 2011

Table 1. Antibacterial Activity of the LL-23 Family against Two *E. coli* Strains

peptide	amino acid sequence[a]	purity (%)	MIC (μM)	
			E. coli DC2[b]	*E. coli* K12[c]
LL-23	LLGDFFRKSKEKIGKEFKRIVQR	96.27	9	160
LL-23A9	LLGDFFRK**A**KEKIGKEFKRIVQR	96.79	9	80
LL-23V9	LLGDFFRK**V**KEKIGKEFKRIVQR	95.20	2	40
LL-37	LLGDFFRKSKEKIGKEFKRIVQRIKDFLRNLVPRTES	97.86	3	5
LL-37A9	LLGDFFRK**A**KEKIGKEFKRIVQRIKDFLRNLVPRTES	99.02	6	15
LL-37V9	LLGDFFRK**V**KEKIGKEFKRIVQRIKDFLRNLVPRTES	99.67	12	25

[a]Altered amino acid residues (in single-letter code) are underlined and bold. [b]DC2 is a supersusceptible *E. coli* strain with the outer membrane altered.[23] [c]Measured as described previously.[18]

To study the structure−activity relationships of the natural fragments of human LL-37, which are poorly understood, we established bacterial expression systems for LL-23, LL-29, and KS-30. While LL-29 and KS-30 were found to be moderately antibacterial, LL-23 was poorly active (MIC > 150 μM) against *Escherichia coli* K12.[17] The structural basis for the poor antimicrobial activity of LL-23 has not yet been explained. In addition, the poor antibacterial activity of LL-23 suggests that it may have other functional roles. To provide insight into different membrane-mimetic models, we compared the NMR structure and dynamics of LL-23 in the micelles of dodecylphosphocholine (DPC), sodium dodecyl sulfate (SDS), and dioctanoylphosphatidylglycerol (D8PG). Because the results in DPC and D8PG are more similar, and deuterated D8PG is not yet commercially available, we determined the three-dimensional (3D) structure of LL-23 in complex with deuterated DPC micelles by NMR spectroscopy. A unique hydrophilic residue, Ser9, was found on the hydrophobic surface of the 3D structure of micelle-bound LL-23. Interestingly, the same position in the sequences of homologous cathelicidins from primates is occupied by an Ala or Val residue.[18] To substantiate the essential role of Ser9, we created single-amino acid residue variants of LL-23 by changing Ser9 to Ala or Val (Table 1). Because the N-terminal region of LL-37 is implicated in chemotaxis, we also evaluated the immunomodulatory activities of LL-23. Our studies revealed that position 9 of LL-23 is essential in regulating the immune and antimicrobial roles of the peptide. We observed that these natural amino acid variations at residue 9 of LL-23 had a dramatic effect on immunomodulatory properties, opening the door to engineering novel immune modulating peptides using a short fragment of LL-37 as a template. Here we report the structure, dynamics, antimicrobial activity, and immune regulation of LL-23 and its single-amino acid variants generated on the basis of non-human primate cathelicidin homologues.

MATERIALS AND METHODS

Peptides. For biological studies, all the peptides (Table 1) were chemically synthesized at isotopic natural abundance and purified to homogeneity (>95% pure) by reverse-phase high-performance liquid chromatography (HPLC) (Genemed Synthesis, Inc.). The C-termini of these peptides were not amidated. In addition, ^{15}N-labeled LL-23 was expressed in *E. coli* and purified using the established protocol.[17] The recombinant form of LL-23 contained an additional Pro residue at the N-terminus of the peptide, which resulted from formic acid cleavage of the Asp-Pro site in the fusion protein created to release the peptide. Previous studies showed that this additional Pro had no effect on antibacterial activity against *E. coli*.[17]

Antimicrobial Activity Assays. The antibacterial activities of LL-23 and its variants were determined using the standard broth microdilution method as described previously.[19] In brief, a 5 mL culture was grown overnight. A fresh culture (5 mL) was inoculated with a small aliquot of the overnight culture and incubated at 37 °C (250 rpm) until the optical density was approximately 0.5. The culture was then diluted to ~10^6 colony forming units (CFU) per milliliter, and 90 μL aliquots were placed in a 96-well microplate. The bacteria were treated with a series of peptide solutions (10 μL) with 2-fold dilution. The assays were performed in triplicate for each peptide. The plate was incubated at 37 °C overnight (~16 h) and read on a ChroMate 4300 Microplate Reader at 630 nm (GMI, Ramsey, MN). The minimal inhibitory concentration (MIC) was defined as the lowest peptide concentration that fully inhibits bacterial growth.[19] In addition, the effect of carbonate anion on peptide activity was evaluated to better mimic physiological conditions.[20] Finally, the modified Clinical and Laboratory Standards Institute protocol for antibacterial assays used in initial testing was described previously.[21] The method was modified to prevent binding of the peptide to plastic.

The minimal bactericidal concentration (MBC) was determined by taking the wells just above the MIC (i.e., those that showed inhibition) and plating them for viable colonies. The MBC is the concentration at which no viable colonies can be obtained.

Immunomodulatory Assays. Venous blood from healthy volunteers was collected in Vacutainer collection tubes containing sodium heparin as an anticoagulant (BD Biosciences) in accordance with University of British Columbia ethical approval and guidelines. Isolation of peripheral blood mononuclear cells (PBMC), assessment of potential cytotoxicity by lactate dehydrogenase (LDH) release, stimulation of cells with peptides and bacterial lipopolysaccharide (LPS), and measurement of cytokine release by an ELISA were all performed exactly as described previously.[22]

Membrane Potential Measurements. Cytoplasmic membrane permeabilization was assessed by using the membrane potential sensitive cyanine dye diS$C_3$5.[23] The mutant *E. coli* DC2 with increased outer membrane permeability was used so that diS$C_3$5 could reach the cytoplasmic membrane.

NMR Sample Preparations. For structural and dynamic characterization by heteronuclear NMR spectroscopy, ^{15}N-labeled LL-23 and lipids were solubilized in 300 μL of water containing 10% D_2O as the field-locking signal. In the final sample, the peptide concentration was ~0.5 mM. The LL-23:lipid molar ratios were 1:20, 1:60, and 1:60 for protonated D8PG (Avanti Polar Lipids, Alabaster, AL), deuterated SDS, and deuterated DPC (Cambridge Isotope Laboratories, Andover, MA), respectively. The solution was transferred to a SHIGEMI (Tokyo, Japan) tube for NMR measurements. For determination of three-dimensional structure, NMR samples in

dx.doi.org/10.1021/bi2016266 | *Biochemistry* 2012, 51, 653−664

300 μL of a 90% H_2O/10% D_2O solution contained 2 mM synthetic peptide (LL-23, LL-23A9, or LL-23V9) and 120 mM deuterated DPC (pH 5.4). These unlabeled samples were used to collect both two-dimensional (2D) proton NMR spectra and HSQC spectra at natural abundance. For proton−deuterium (H−D) exchange experiments, the samples of LL-23, LL-23A9, and LL-23V9 described above bound to DPC micelles were dried and resolubilized in 99.9% D_2O followed by immediate NMR measurements.

Translational Diffusion Coefficient Measurements. Translational diffusion coefficients (D_f) are inversely proportional to the size of the particle. In particular, the D_f of a peptide changes substantially upon association of the peptide with membrane-mimetic micelles.[24] The D_f values for synthetic LL-23 and its variants in complex with micelles were measured at 25 °C on a 400 MHz Bruker NMR spectrometer using the 2D DOSY technique.[25]

Multidimensional NMR Spectroscopy. For 2D homonuclear ^{1}H NMR studies of unlabeled peptides, a set of spectra, including NOESY, TOCSY, and DQF-COSY,[26−28] was recorded for signal assignments at 25 °C. To confirm the assignments, data were also collected at 35 °C. The ^{1}H spectral width in both dimensions was 8510.6 Hz. To verify the proton assignments and to further refine the structure,[29] gradient-enhanced HSQC spectra,[30] between ^{1}H and ^{15}N, or between ^{1}H and ^{13}C, were also recorded for 2 mM synthetic LL-23 or its variants at natural abundance. The ^{1}H, ^{15}N, and ^{13}C carriers were set at 4.77, 118.27, and 36.37 ppm, respectively. Typically, 30 increments (128 scans) and 80 increments (256 scans) were collected for the ^{15}N (spectral width of 2200 Hz) and aliphatic ^{13}C (spectral width of 12000 Hz) dimensions, respectively.

For multidimensional heteronuclear NMR studies, ^{15}N-labeled recombinant LL-23 was utilized. 2D HSQC spectra were recorded at a sweep width of 2200 Hz with 100 increments. For signal assignments, 3D ^{15}N-edited NOESY-HSQC and TOCSY-HSQC spectra were collected.[31] Residue-specific heteronuclear ^{15}N{^{1}H} NOE values for LL-23 in complex with different micelles were obtained from 2D (^{1}H and ^{15}N) HSQC spectra with and without proton saturation. The ^{15}N longitudinal and transverse relaxation times (T_1 and T_2, respectively) of LL-23 were measured by integrating the proton peaks over the entire amide region. The relaxation delays used for measuring T_1 were 0, 0.05, 0.13, 0.25, 0.51, 1, and 2 s, while the relaxation delays used for measuring T_2 were 0.01, 0.03, 0.09, 0.19, 0.35, 0.41, and 0.49 s. Chemical shifts were referenced as described previously.[32] Data were recorded on a 600 MHz Varian INOVA NMR spectrometer equipped with a triple-resonance cryogenic probe with a *z*-axis gradient capability. These data were then transferred to and processed off-line on a Silicon Graphics Octane workstation using NMRPipe and analyzed by PIPP.[33,34]

Three-Dimensional Structures of the Peptides in Membrane-Mimetic Micelles. For structural calculations of LL-23, LL-23A9, and LL-23V9, the major restraints were derived from 2D NOESY spectra.[35] For LL-23, additional distance restraints were obtained from 3D ^{15}N-separated NOESY spectra. The cross-peaks were integrated by PIPP and converted to distance restraints of 1.8−2.8, 1.8−3.8, 1.8−5.0, and 1.8−6.0 Å, corresponding to strong, medium, weak, and very weak types of NOE peaks, respectively. On the basis of ^{1}Hα, natural abundance ^{15}N, ^{13}Cα, and ^{13}Cβ chemical shifts, backbone angles were predicted by using an updated version of TALOS.[36] Hydrogen bond restraints were introduced on the basis of H−D exchange experiments, temperature coefficients, and the NOE-derived structures.[18] An extended covalent structure was used for the starting coordinates. An ensemble of 100 structures was calculated by using the simulated annealing protocol in Xplor-NIH.[37] Twenty structures were accepted on the basis of the following criteria: no NOE-derived distance violations of >0.20 Å, back dihedral angle violations of <2°, rmsd for bond deviations from ideality of <0.01 Å, and rmsd for angle deviations from ideality of <5°. The structures were viewed and analyzed using MOLMOL[38] and PROCHECK.[39] The 20 structures and ^{1}H, ^{13}C, and ^{15}N chemical shifts of human LL-23 bound to DPC micelles were deposited in the Protein Data Bank (PDB entry 2LMF) and BioMagResBank (BMRB entry 18114).

RESULTS

Antibacterial Activity of LL-23 and Its Variants. Initially, antimicrobial activities were evaluated as MIC against wild-type *E. coli* K12 using a previously described protocol.[18] The MIC decreased from LL-23 to LL-23A9 to LL-23V9, indicating that the type of residue at position 9 influenced peptide activity (Table 1). To substantiate these small differences in MIC, we utilized a more sensitive *E. coli* strain, DC2, which has a decreased outer membrane permeability barrier and is consequently supersusceptible to peptides.[23] LL-23 was found to inhibit this supersusceptible strain at 9 μM, a value only 3-fold increased over the MIC of LL-37 against this same strain (Table 1), indicating that the outer membrane permeability barrier explained in part the very poor ability of LL-23 to kill wild-type *E. coli*. When residue Ser9 was altered to Ala9 (i.e., LL-23A9), a similar MIC was found. A substantial increase in MIC was observed for the LL-23V9 variant (2 μM). For comparison, we also determined the MICs of LL-37 and the corresponding single-residue variants using both supersensitive and wild-type *E. coli* strains. Interestingly, the MIC increased slightly from LL-37 to LL-37A9 to LL-37V9 (Table 1).

We also measured the antimicrobial activities of LL-23 and its single-residue variants against the Gram-positive *Staphylococcus aureus* UAMS-1, a clinical isolate, and found it to be inactive (MIC > 160 μM). Consistent with this observation, LL-23 and its variants (Table 2) displayed no activity against a wild-type *S. aureus* Rosenbach strain. In the presence of carbonate, only LL-23V9 showed a slightly reduced MIC (12 μM). To better delineate the activity differences of these peptides, we tested a cationic peptide-susceptible *S. aureus* strain, with an *mprF* mutation (Table 2). The MICs of both LL-23A9 and LL-23V9 were reduced by 4-fold compared to that of LL-23 (24 μM). In the presence of physiologically relevant carbonate,[20] the bacterium became even more susceptible with the MICs decreased to the 0.35−0.7 μM range for the Ala and Val variants of LL-23. We also measured the minimal bactericidal concentrations (MBCs). While the wild-type *S. aureus* strain was not killed at an MBC of >24 μM, the LL-23 variants were able to kill the *mprF* strain of *S. aureus* at 3−12 μM. Although the antimicrobial activity of these peptides depended on both bacterial strains and medium conditions (Tables 1 and 2), it is evident that LL-23V9 was more active than LL-23 while LL-23A9 was equivalent versus *E. coli* DC2 and more active versus *E. coli* K12 or *S. aureus*.

Chemokine Release and Cytotoxicity. The immunomodulatory activities of the LL-23 variants were tested using PBMC. Previous studies have demonstrated that there are two major immunomodulatory activities of cationic peptides that

Table 2. Activities of LL-23 and Its Variants against *S. aureus*

	MIC (μM)				MBC (μM)			
	WT[a]		*mprF* mutant[a]		WT[a]		*mprF* mutant[a]	
peptide	−C[b]	+C[b]	−C[b]	+C[b]	−C[b]	+C[b]	−C[b]	+C[b]
LL-23	>24	>24	24	3	>24	>24	>24	12
LL-23A9	>24	>24	6	0.35−0.7	>24	>24	6−12	6
LL-23V9	>24	12	6	0.35−0.7	>24	>24	3−6	6−12

[a]WT, wild-type *S. aureus*; *mprF* mutant with multiple peptide resistance genes knocked out.[62] [b]The assay culture contains physiological concentrations of carbonate that generally enhance the susceptibility to cationic AMPs.[20] In the table, +C denotes the presence of carbonate and −C the absence of that salt.

correlate with protection in animal models, namely, their ability to attract immune cells through the production of chemokines like MCP-1 (CCL2) and their ability to suppress the production of pro-inflammatory cytokines like TNF-α in response to bacterial signature molecules like LPS.[40,41] This selective modulation of innate immunity does not per se result in cytotoxicity, and we confirmed here that none of the LL-23 peptides or LPS utilized led to more than 4% of the maximal release of cytosolic lactate dehydrogenase in PBMC.

To assess their immunomodulatory activities, we evaluated cytokine and chemokine release in the presence of LL-23 and its variants and compared the results with those of LL-37 and its single-amino acid substitution variants (Figure 1). The LL-37 variants were identical to LL-37 in demonstrating no induction of the pro-inflammatory cytokine TNF-α, a moderate ability to induce chemokine MCP-1 (cf. treatment with LPS) and a strong ability to suppress LPS-induced TNFα while maintaining the level of induced MCP-1.[22,42] In contrast, LL-23 was able to induce moderate levels of MCP-1 but lacked the ability to suppress the release of LPS-induced MCP-1 or TNF-α. However, alteration of Ser9 of LL-23 to either Ala or Val restored the ability to reduce the level of LPS-mediated TNF-α release but had contrasting effects on MCP-1 production. Thus, LL-23V9 failed to induce any MCP-1 by itself and strongly suppressed LPS-induced MCP-1 production, indicating that it was a potent anti-inflammatory peptide, while LL-23A9 by itself induced MCP-1 induction but, unlike LL-37 or LL-23, strongly maintained LPS-induced chemokine production.

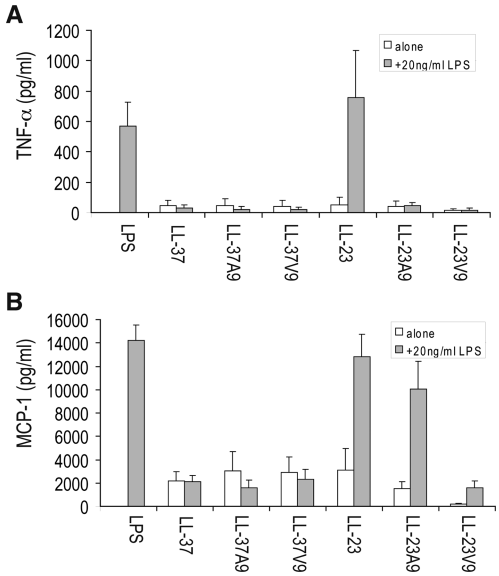

Figure 1. Production of pro-inflammatory cytokine TNF-α (A) or chemokine MCP-1 (CCL2) (B) in response to peptides in the presence or absence of bacterial LPS. Human PBMC were treated with 20 μg/mL peptide in the presence or absence of 20 ng/mL LPS, and after 24 h, the production of TNF-α or MCP-1 was assessed by an ELISA. The data in panel A demonstrate that none of the peptides was intrinsically pro-inflammatory and only LL-23 failed to suppress LPS-mediated TNF-α production. The data in panel B demonstrate that all of the peptides except LL-23V9 were able to induce substantial levels of baseline MCP-1 but differed in their ability to suppress LPS-mediated MCP-1 production. Results represent the means ± SD of five experiments.

Membrane Depolarization. To provide insight into the antimicrobial mechanism of action, we measured the effects of the peptides on bacterial membrane potential in the supersusceptible *E. coli* DC2 mutant.[23] The fluorophore diSC$_3$5 is a caged cation that is concentrated within the cytoplasmic membrane of bacteria under the influence of the bacterial membrane potential gradient ($\Delta\psi$); at these high concentrations, it self-quenches, leading to a suppression of fluorescence. When the membrane becomes leaky for cations, including protons, the $\Delta\psi$ is dissipated, leading to release of diSC$_3$5. As shown for other cationic peptides, LL-37 showed a concentration-dependent fluorescence increase from 3 to 12 μM (Figure 2), indicating that this peptide was permeabilizing the membrane. At the same peptide concentrations, similar effects were observed with LL-23 and its variants in this supersusceptible strain, indicating that LL-23 did have the potential to act on bacterial membranes and reinforcing the idea that poor permeability across the outer membrane was the basis for the poor activity of this peptide against *E. coli*. Interestingly, LL-23A9 and LL-23V9 displayed increased permeability, and the membrane permeability of LL-23V9 was comparable to that of LL-37 in this model bacterium (Figure 2).

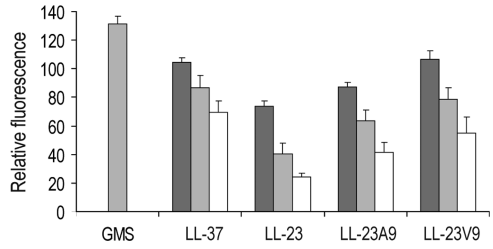

Figure 2. Depolarizing activity of the LL-37-derived peptides. The *E. coli* DC2 susceptible strain was used in these experiments.[23] The percent dequenching of fluorescence of the membrane-potential sensitive fluorophore diSC$_3$5 was assessed as a function of peptide concentrations of 8 (white bars), 16 (light gray bars), and 32 μg/mL (dark gray bars). These concentrations correspond to 3, 6, and 12 μM for the LL-23 series and 2, 4, and 8 μM in the case of LL-37, respectively. As a positive control, gramicidin S (GMS) was used at 16 μg/mL.

dx.doi.org/10.1021/bi2016266 | *Biochemistry* 2012, 51, 653−664

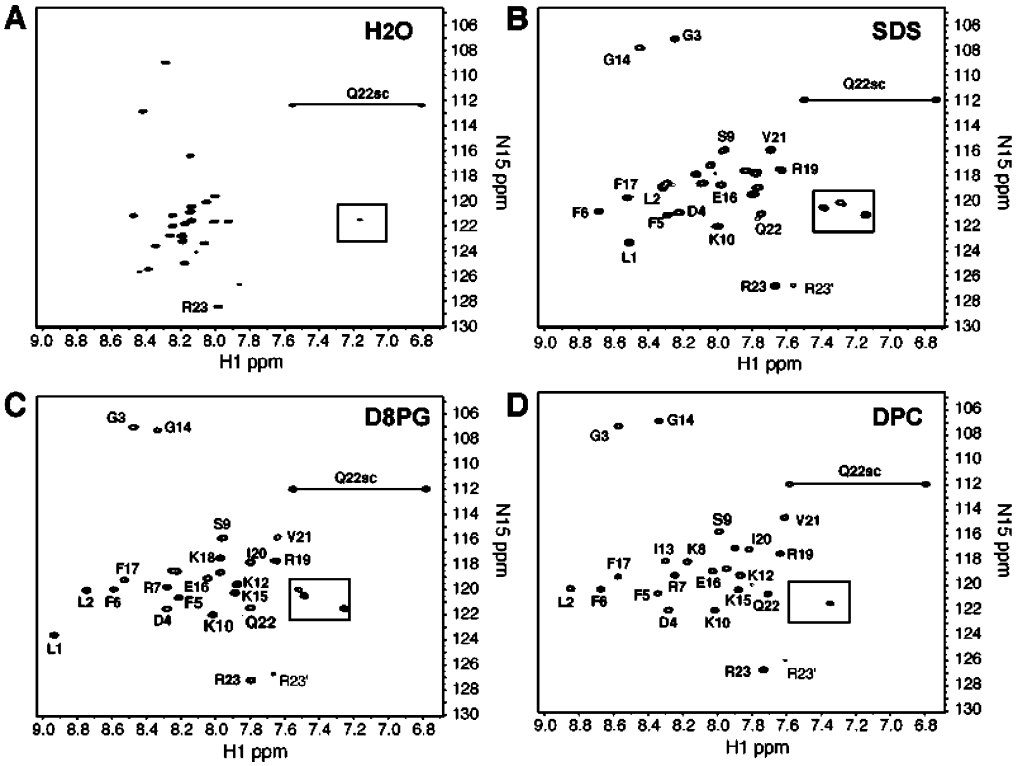

Figure 3. HSQC spectra of ^{15}N-labeled LL-23 in water (A) or in a complex with (B) SDS, (C) D8PG, or (D) DPC at pH 6 and 35 °C. The peptide concentration was ~0.5 mM (1.5 mg/mL). For peptide:lipid ratios and other data, see Table 3. For the sake of clarity, peaks are partially labeled. There are two sets of peaks for R23. Side chain signals are boxed or connected by a line.

Effects of Micelle Type on the Structure and Backbone Dynamics of ^{15}N-Labeled LL-23. To provide atomic insight into the interactions of the peptide with different membranes, we conducted NMR studies of ^{15}N-labeled LL-23 in three membrane-mimetic micelles: SDS, DPC, and D8PG. While deuterated SDS and DPC are widely utilized,[35] D8PG is a newly established model.[18,43] D8PG possesses a phosphatidylglycerol headgroup, identical to the native anionic lipids in bacterial membranes. In water, the cross-peaks of ^{15}N-labeled LL-23 occupied a narrow range of 7.9−8.5 ppm in the proton dimension, indicating a random coil conformation (Figure 3A). The cross-peaks of the peptide expanded to a wider range of approximately 7.6−8.9 ppm in the presence of micelles (Figure 3B−D). In addition, the cross-peaks of the peptide became broader. These observations indicated the binding of the peptide to membrane-mimetic micelles and folding into an ordered structure.[44] To provide additional evidence of complex formation, we measured the T_1 and T_2 relaxation times of the peptide in the absence or presence of micelles.[18] On the basis of the T_1/T_2 ratios, the correlation times (τ_c) of the peptide with and without micelles were calculated (equation in Table 3). The τ_c is related to the size of the molecular system under investigation. In water, LL-23 had a τ_c of 3.5 ns. In the presence of micelles, the correlation times doubled (6.3−7.0 ns). The τ_c values of the peptide in the bound state were comparable to those previously measured for small proteins,[45] indicating the formation of a complex between the peptide and micelle in each case. While the τ_c values of the LL-23 peptide measured in SDS and DPC micelles were essentially identical, the value was slightly larger in D8PG micelles (Table 3). It appeared that the peptide−D8PG complex was slightly larger than the complex of the peptide with either SDS or DPC.

Table 3. NMR Characterization of ^{15}N-Labeled LL-23 in Water or Bound to Micelles

detergent or lipid	peptide:lipid ratio[a]	T_1 (ms)[b]	T_2 (ms)[b]	τ_c (ns)[c]
water[d]	1:0	804	427	3.5
SDS	1:60	645 ± 6	165 ± 3	6.3 ± 0.1
DPC	1:60	669 ± 21	169 ± 11	6.4 ± 0.1
D8PG	1:20	711	154	7.0

[a]All the measurements were taken at pH 6 and 35 °C. [b]Exponential fits to obtain T_1 and T_2 for each case are of high quality as reflected by a correlation coefficient of ≥0.99. [c]The correlation time (τ_c) was calcualted on the basis of relationship $T_1/T_2 \approx 0.5\omega_o^2\tau_c^2$ for proteins (<25 kDa), where the angular velocity $\omega_o = 2\pi\upsilon_o$ and υ_o is the precession frequency of ^{15}N (60.785 MHz on our 14.1 T magnet).[63] [d]Measurements were duplicated in SDS or DPC, but not in water or D8PG.

Chemical shifts are sensitive to protein conformation. Therefore, the H^α chemical shifts of LL-23 in SDS, DPC, or D8PG micelles were compared in Figure 4A. Nearly identical H^α chemical shifts supported similar backbone conformations of the peptide in these micelles. To provide site-specific insight into the backbone dynamics of LL-23 in these model systems, we measured heteronuclear ^{15}N NOEs for each residue of LL-23 in these micelles. In both DPC and D8PG micelles, Figure 4B indicates that LL-23 was rigid from residue 2 to 20 (^{15}N NOE ~ 0.6−0.8). There were larger motions for residues 21 and 22, and residue 23 appeared to be more mobile as indicated by a small or negative ^{15}N NOE. In SDS, residues 2 and 3 were moderately mobile (^{15}N NOE = 0.2−0.5) followed by a rigid helical region between residues 4 and 20. Nevertheless, the motion pattern for residues 21−23 of the peptide in SDS was similar to those observed in DPC or D8PG micelles.

dx.doi.org/10.1021/bi2016266 | *Biochemistry* 2012, 51, 653−664

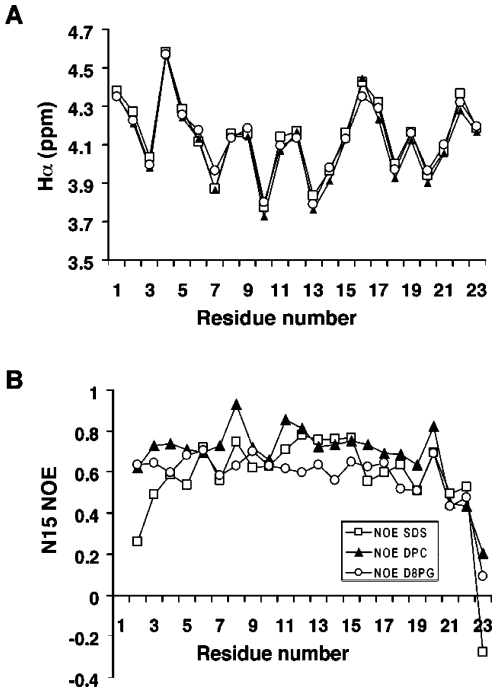

Figure 4. Structure and dynamics of ^{15}N-labeled LL-23 in complex with SDS, D8PG, or DPC micelles. (A) H$^{\alpha}$ chemical shift plot of LL-23 in SDS (□), D8PG (○), or DPC (▲). (B) ^{15}N NOE values of LL-23 measured in complex with SDS, D8PG, or DPC micelles under the conditions described in the legend of Figure 3.

Note that the C-terminal backbone ^{15}N nucleus of Arg23 showed an increased level of motion from DPC to D8PG to SDS micelles (Figure 4B). This was likely due to stronger charge repulsion between the negatively charged C-terminal end of LL-23 and the headgroup of the micelles from DPC (neutral) to D8PG (anionic) to SDS (strongly anionic).[46] A different micelle-dependent phenomenon was demonstrated for the N-terminus of the peptide. The strong headgroup of SDS made the micelle surface more acidic,[47] leading to a strong cross-peak for Leu1 (visible because of a precedent Pro residue in the recombinant construct) in SDS, moderate in D8PG, and too weak to be detected in DPC because of rapid exchange at pH 6 (Figure 3). Meanwhile, the N-terminal amide protons for residues L1, L2, and G3 shifted upfield in SDS (Figure 3B) compared to those in D8PG or DPC (Figure 3C,D), leading to an improved spectral dispersion of those protons in the latter two systems. Dynamically, however, the peptide behaved more similarly in DPC and D8PG micelles (Figure 4B). In addition, the HSQC spectral dispersions and peak positions of LL-23 in DPC and D8PG were also more comparable (Figure 3). These results indicated that DPC might be more similar to D8PG than SDS. Because deuterated D8PG is not yet commercially available, we utilized deuterated DPC micelles below as a model for high-quality structural determination of LL-23 and its variants in the membrane-bound state.

Three-Dimensional Structures of LL-23, LL-23A9, and LL-23V9 in Complex with DPC Micelles. The T_1/T_2 ratio-based method described above for calculating correlation times requires isotope labeling of AMPs. In the absence of isotope labeling, translational diffusion coefficients (D_f) can be measured as an indication of complex formation whereby the larger the complex, the slower its diffusion.[24] The diffusion coefficient for the peptide alone in solution was 1.6×10^{-6} cm^2/s, whereas LL-23, LL-23A9, and LL-23V9 in the presence of DPC micelles all had diffusion coefficients around 1.0×10^{-6} cm^2/s, indicating the formation of a complex in all cases.[24]

Sequential NMR signal assignments for LL-23 or its variants in complex with DPC micelles were achieved by using the established 2D NMR method.[35] In brief, amino acid spin systems were identified in the TOCSY spectrum followed by the establishment of their connectivities via the NOESY spectrum. In each case, the NOE patterns in the fingerprint region contained (i,i+3) and (i,i+4) types of connectivities, typical of helical structures. TALOS[36] analysis of ^{1}Hα, ^{15}N, ^{13}Cα, and ^{13}Cβ chemical shifts of micelle-bound peptides identified a helical region spanning residues 2−21 for LL−23 and its single-residue variants. The NMR restraints used for determining the 3D structures of LL-23 and its variants are summarized in Table 4. Figure 5 presents an ensemble of 20 structures for each peptide accepted using the criteria defined in Materials and Methods. The root-mean-square deviations were 0.39, 0.62, and 0.36 Å for LL-23 (A), LL-23A9 (C), and LL-23V9 (E), respectively, when the backbone atoms of residues 2−20 were superimposed. A Procheck analysis[39] of the ensemble of structures showed that 89.5−94.7% of the residues of these peptides are located in the most favored region of the Ramachandran plot (Table 4). Thus, these structures were determined to high quality. Detailed statistics for each structural ensemble are summarized in Table 4. As shown in the ribbon diagram of the peptide structure, the hydrophobic surface of LL-23 was segregated by a hydrophilic residue Ser9 (Figure 5B), whereas both LL-23A9 and LL-23V9 possessed continuous hydrophobic surfaces (Figure 5D,F). The continuity of the hydrophobic surfaces (in green) in the case of the LL-23 variants was evident in the colored space-filling models

Table 4. Structural Statistics of Human LL-23 and Its Mutants in DPC Micelles

	LL-23	LL-23A9	LL-23V9
structural restraints			
no. of NOE restraints (total)	255	217	257
intraresidue	74	73	54
sequential	89	76	86
short-range	89	68	117
no. of backbone angles (ϕ/ψ)[a]	38	42	42
structure and quality			
helical region	2−20	2−20	2−21
helicity based on structure (%)	83	83	87
helicity based on H$^{\alpha}$ chemical shifts (%)	78	77	79
backbone rmsd (Å)[b]	0.39	0.62	0.36
NOE-derived distance violations (Å)	<0.5	<0.5	<0.5
TALOS-derived angle violations (deg)	<5	<5	<5
Ramachandran plot[c]			
residues in the most favored region (%)	89.5	89.5	94.7
residues in the additional allowed region (%)	10.5	10.5	5.3

[a]Predicted by the updated version of TALOS.[36] [b]Calculated with MOLMOL[38] when the backbone atoms of residues 2−20 of the accepted ensemble of 20 structures are superimposed. [c]Calculated with Procheck.[39]

dx.doi.org/10.1021/bi2016266 | Biochemistry 2012, 51, 653−664

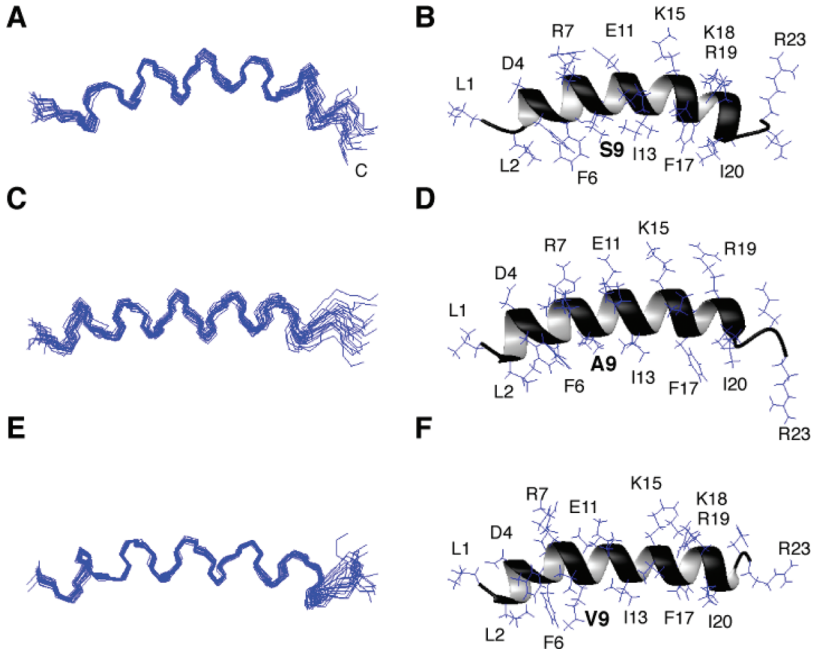

Figure 5. Solution structures of human LL-23 and its single-residue variants in complex with deuterated DPC at pH 5.4 and 25 °C. Shown are ensembles of 20 backbone structures of LL-23 (A), LL-23A9 (C), and LL-23V9 (E) with amino acid residues 2−20 superimposed and ribbon diagrams of LL-23 (B), LL-23A9 (D), and LL-23V9 (F) with side chains labeled. In panels B, D, and F, the residue at position 9 is shown in bold.

in Figure 6. Interestingly, a similar hydrophobic gap exists in the 3D structure of intact LL-37 bound to SDS micelles (Figure 7A).

Hydrogen−Deuterium Exchange Dynamics Explains Peptide Activity Differences. Because the 3D structures of LL-23, LL-23A9, and LL-23V9 were similar, we also investigated the dynamic aspect of these peptides bound to DPC micelles based on H−D exchange experiments. This was performed by removing the water in the NMR samples followed by adding the same volume of deuterium oxide. As a consequence of H−D exchange, those exchangeable proton signals of the peptides became weaker and eventually disappeared from proton-detected NMR spectra. In the case of LL-23, the amide proton signals of terminal residues 2−5, 22, and 23 disappeared in 20 min. After 21 h, only the backbone amide proton signals for residues I13, F17, and I20 of the peptide remained (Table 5). All the backbone amide signals of LL-23 disappeared within 6 days. After 21 h, for LL-23A9, only the amide proton signals of A9, K10, I13, and F17 were detected, while in the case of LL-23V9, only the peaks for V9, K10, K12, I13, and F17 were detected. After 72 h, only the peaks of I13 and V9 of LL-23V9 remained. The signal of I13 was even observed for LL-23A9 and LL-23V9 after 2 weeks. Overall, there was a trend of slowed exchange of an increasing number of residues from LL-23 to LL-23A9 to LL-23V9 after 21 h (Table 5). The slowed exchange of the amide protons of the LL-23 variants might reflect their deeper penetration into the DPC micelles. The enhanced membrane penetration ability from LL-23 to LL-23A9 to LL-23V9 was in line with their increased peptide hydrophobicity according to HPLC retention times (Table 5).[49] Remarkably, the exchange dynamics of LL-23 and its variants were fully consistent with their antimicrobial activities. We propose that deeper penetration of LL-23V9 into the bacterial cytoplasmic membrane was important for its enhanced antibacterial activity against both the supersusceptible and normal strains of Gram-negative *E. coli* (Table 1).

DISCUSSION

This study provided unique insight into the structure, dynamics, and functions of LL-23, a natural derivative of human cathelicidin LL-37, and of the differential activities of hypothesized primate variants. The structure and dynamics of LL-23 were similar in SDS, DPC, and D8PG micelles, indicating that these membrane-mimetic micelles had little impact on the peptide conformation. A helical structure was found between residues 2 and 20 of the peptide with the three C-terminal residues disordered. The increased levels of motion at the C-terminus of LL-23 could be attributed to peptide chain truncation, as these residues are structured in intact LL-37 (Figure 7B). Mobile residues were also observed at the C-terminus of LL-37, and they were not required for membrane binding (Figure 7). Except for the disordered C-terminus, the LL-23 structure in DPC micelles was identical to that in the high-resolution structure of intact LL-37 bound to SDS micelles (Figure 7). The fact that both the structures of LL-23 (this study) and LL-37[18] were independent of micelle types led us to conclude that the differences between the two LL-37 structures, one determined in DPC micelles by 2D NMR[48] and the other in SDS micelles determined by 3D NMR,[18] might stem from the insufficient spectral resolution in the 2D NMR case as initially noted by Li et al.[49] In the high-resolution structures of both SDS-bound LL-37 and DPC-bound LL-23 (Figure 7), the helix started from residue 2 and the aromatic rings of F5 and F6 were perpendicular to each other as a result of aromatic−aromatic interactions.

Interestingly, determination of structure revealed a hydrophobic defect in the structure of LL-23, whereby a hydrophilic Ser9 segregated the hydrophobic surface into two clusters (Figure 6). However, there was no increased level of motion at Ser9 based on heteronuclear ^{15}N NOE measurements (Figure 4B). Therefore, the poor activity of LL-23 was not due to an increased level of motion at that position on the picosecond to nanosecond time scale. Similar results were observed in the

dx.doi.org/10.1021/bi2016266 | *Biochemistry* 2012, 51, 653−664

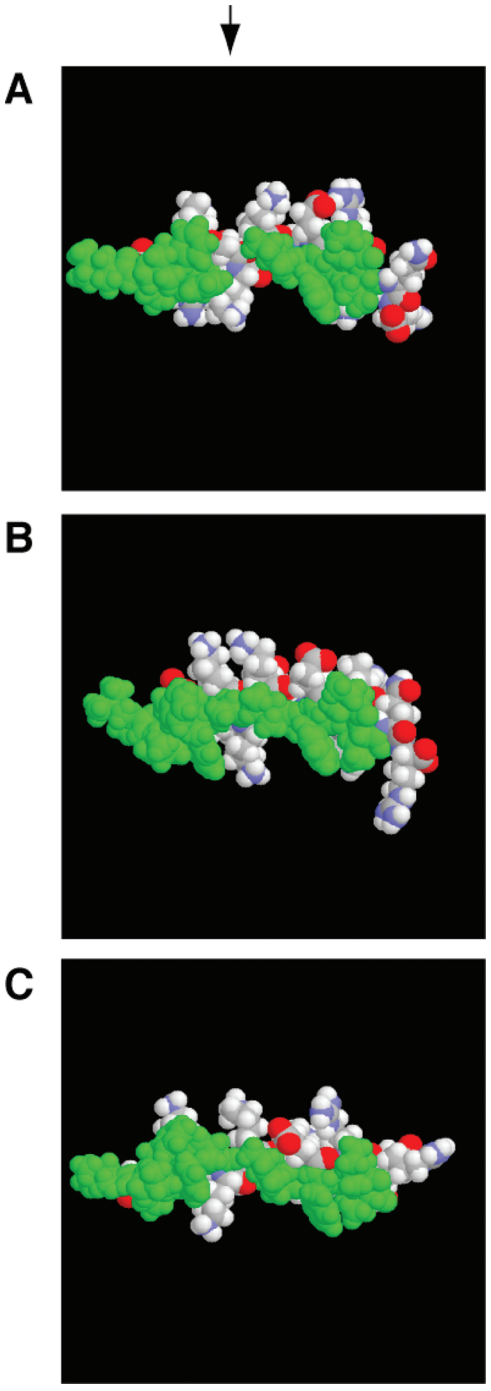

Figure 6. Space-filling models of LL-23 (A), LL-23A9 (B), and LL-23V9 (C) in complex with membrane-mimetic DPC micelles. Color code: red for oxygen, blue for nitrogen, white for carbon and hydrogen, and green for hydrophobic side chains. The hydrophobic defect at residue Ser9 of LL-23 (arrow) is a hot spot, which formed the basis for structure-based peptide design in panels B and C.

high-quality structure of intact LL-37 (Figure 7A).[18] Zelezetsky and colleagues sequenced cathelicidins from more than a dozen primates.[50] Sequence comparison revealed that at position 9, human LL-37 possesses a Ser residue, while the same position in non-human primate cathelicidins has an Ala or Val residue.[18] Our results indicated that a change of hydrophilic Ser9 on the hydrophobic surface of LL-23 to hydrophobic Ala or Val did not change the backbone structure of the peptide (Figure 5). Thus, the activity differences of LL-23 and its variants could not

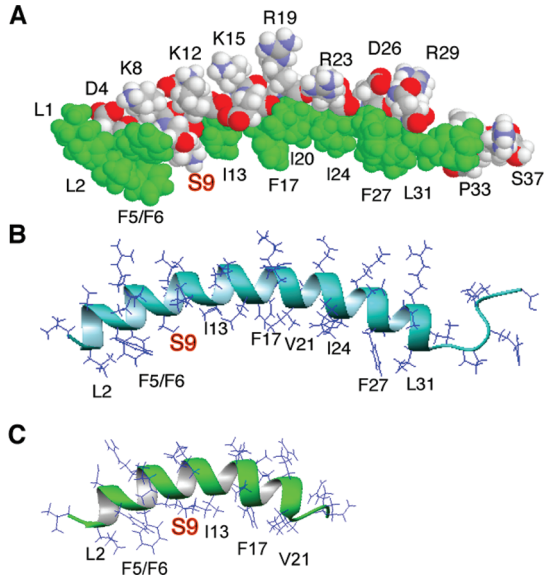

Figure 7. Structural comparison of human LL-37 with LL-23 in complex with micelles. The structure of LL-37 (PDB entry 2K6O) was reported previously.[18] The space-filling and ribbon diagram models of LL-37 are shown in panels A and B, respectively, while a ribbon diagram of LL-23 (PDB entry 2LMF) is shown in panel C. Both LL-37 and LL-23 consist of an amphipathic helix followed by a short disordered tail at the C-terminus. Note that only the amphipathic helix portion is required to associate with bacterial membranes. Also in both structures, a hydrophilic Ser9 (gold) is located on the hydrophobic surface, leading to two hydrophobic domains in each. The two-domain structure[18] explains the cooperative LPS binding of LL-37[56] and weak LPS binding of LL-23 (see the text).

Table 5. Summary of H−D Exchange Results of Amide Protons in Three Peptide/DPC Micelles after 21 h

peptide	sequence pattern of slowly exchanged amides (bold and underlined)	no. of amides detected	HPLC retention time (min)[a]
LL-23	LLGDFFRKSKEK**I**GKE**F**KR**I**VQR	3	9.702
LL-23A9	LLGDFFRK**AK**EK**I**GKE**F**KRIVQR	4	10.331
LL-23V9	LLGDFFRK**VK**E**KI**GKE**F**KRIVQR	5	10.817

[a]The retention time of the peptide was measured on a Waters HPLC system equipped with an analytical reverse-phase Waters symmetry C8 column (150 mm × 3.9 mm). The peptide detected at 215 nm was eluted with a gradient of acetonitrile (containing 1% TFA) from 5 to 95% at a flow rate of 1 mL/min.

be explained at the backbone level of the 3D structure in this case. This observation revealed the challenge in correlating the 3D structure of AMPs with antimicrobial activity. What then was responsible for the activity difference? We observed that the H−D exchange rates were reduced when Ser9 of LL-23 was substituted with Ala or Val. Therefore, the existence of hydrophilic Ser9 on the hydrophobic surface did not allow LL-23 to penetrate as deeply into the membrane environment, consistent with its poor ability to kill even supersusceptible or carbonate-treated bacteria (Table 1) or polarize the bacterial membranes. In contrast, when hydrophilic Ser9 was substituted with hydrophobic Val, the reduced exchange rate corresponded to higher antimicrobial activity as well as improved membrane polarizing ability (Figure 2). Against wild-type *E. coli* K12, the negligible antimicrobial activity of LL-23 was clearly a function of its poor ability to penetrate the outer membrane and possibly

dx.doi.org/10.1021/bi2016266 | *Biochemistry* 2012, 51, 653−664

its sensitivity to rapid efflux from the cell. When this barrier was overcome by using a supersusceptible strain DC2 with an altered outer membrane, the residual antimicrobial activity of LL-23 could be attributed to a large extent to the hydrophobic gap in the 3D structure. This hydrophobic gap, an inherent structural defect, split the hydrophobic surface of LL-23 into two portions (Figure 6A), thereby weakening its membrane penetration and depolarization ability.

Besides direct microbial killing, LL-37 is known to regulate the immune response. It is now well understood that in addition to surface receptors, LL-37 is able to rapidly traverse into mammalian cells in a manner reminiscent of cell-penetrating peptides[51] and interact with cytoplasmic interaction partners in a manner that determines its immunomodulatory properties.[52] In particular, the N-terminal region of LL-37 is implicated in direct chemokine activity.[53] Unlike the potent anti-inflammatory activity of LL-37, this study showed that LL-23 had a weak ability to suppress the LPS-induced release of either TNF-α or MCP-1, which was restored in the case of the primate-specific sequence variant peptides. This suppression activity of LL-37 is related to its LPS binding ability.[54,55] Our previous NMR characterization mapped the LPS binding region of LL-37 to residues 2−31.[18] Because Ser9 separates the hydrophobic surface of LL-37 into two domains (Figure 7A), our 3D structure explains the cooperative LPS binding observed previously.[56] One such domain was located between residues 15 and 32 of LL-37.[57] Because LL-23 contained the short N-terminal LPS-binding domain and part of the strong LPS-binding domain (Figure 5B), it is not surprising that this peptide was unable to effectively suppress LPS-induced TNF-α release (Figure 1A). However, a change of Ser9 of LL-23 to Ala or Val reduced the level of TNF-α release, presumably by enhancing its LPS binding ability. The continuous hydrophobic surface of the LL-23 variants (Figure 6) might also explain in part the increased level of suppression of LPS-induced release of chemokine MCP-1 (Figure 1B). However, the effects of LL-37 in antagonizing LPS stimulation of pro-inflammatory cytokine expression are only partly dependent on LPS binding.[22,54] Thus, we assume that these effects reflected both the relative ability to bind to LPS and a direct influence on signaling.

Importantly, this series of peptide variants offered very different immunomodulatory activities with LL-23 being able to induce chemokine production but no anti-inflammatory effect, LL-23V9 having a potent anti-inflammatory activity but no chemokine production ability, and LL-23A9 not only having the anti-inflammatory activity and chemokine induction abilities of LL-37 but also being able to maintain the protective chemokine response to LPS. Our studies indicated that these substantially shorter variant peptides not only shared properties with their parent peptide LL-37 but also provided the starting points for optimizing peptides with rather distinct and useful immunomodulatory activities. These important findings opened the door to peptide engineering using LL-23 as a model, which clearly possessed favorable properties compared to those of LL-37 in several aspects. First, LL-23 has a shortened sequence, which is less costly to synthesize. Second, LL-23 exhibited low toxicity to mammalian cells because of sequence truncation that disrupted the strong antimicrobial region of LL-37.[49,58] Third, the short sequence of LL-23 also facilitated detailed immune modulation studies of additional peptide variants. Because these LL-23 variants interacted well with both anionic and neutral membrane mimics, it was tempting to speculate that their differences in membrane interaction dynamics and surface properties are responsible for these properties via the influence of their ability to be taken up into host cells and their interaction with discrete receptors.

In summary, our structure−activity relationship studies provided important insight into the functional roles of LL-23. It is a peptide with weak antimicrobial activity as well as weak suppression of pro-inflammatory cytokine induced by LPS. These poor activities, to a large extent, might be attributable to the segregation of the hydrophobic surface of LL-23 into two small hydrophobic clusters by Ser9 (i.e., a structural hot spot) (Figure 6). It is understandable now that mutations at that hot spot of LL-23 drastically affected peptide activities. Interestingly, similar single-residue variants of LL-37, unlike LL-23, did not show distinct differences in immune modulations (Figure 1). Such differences between LL-23 and LL-37 in response to single-residue changes were not determined by the 3D structures (Figure 7), because the structures for residues 2−21 in both peptides were identical, including the location of hydrophilic Ser9 on the hydrophobic surface (Figures 6A and 7A). Rather, we might attribute the difference to the truncation of the LL-37 sequence that disrupted the strong LPS-binding region.[57] In the presence of that region, the effect of the Ser9 to Val substitution on the immune modulating function of LL-37 could have been masked. In the case of LL-23, the same replacement drastically altered the properties of the molecule as a consequence of the merging of the two isolated and small hydrophobic moieties into a continuous and stronger membrane, endotoxin (LPS), or receptor-binding surface (see Figure 6). Such a sequence difference between LL-23 and LL-37 underscored peptide-dependent functional outcomes even though they share the same structure in the corresponding region.

CONCLUSIONS

The significance of host defense peptide LL-37 to human health is now firmly established. Differential expression of this peptide is associated with a variety of diseases, including cancer.[13,59] The 3D structure of human LL-37 provides insight into its antimicrobial and cooperative LPS binding properties.[18,58] The biology of human LL-37 is further complicated by protease-generated fragments for which structure and function are poorly understood. This heteronuclear NMR study of the structure and dynamics of LL-23 is an important step toward understanding its functional roles. Our results for LL-23 in membrane-mimetic micelles (SDS, DPC, or D8PG) made the trend in NMR chemical shifts, peptide structure, and dynamics more understandable. For example, the magnitude of motion of the C-terminal residue on the picosecond to nanosecond time scale was in the SDS > D8PG > DPC order (Figure 4B), which might be due to stronger negative charge repulsion between the peptide and micelles.

In DPC micelles, LL-23, LL-23A9, and LL-23V9 shared the same helical structure (Figure 5), which made a direct structure−activity correlation unsuccessful at the backbone level. Nevertheless, these peptides differed at a critical side chain, which was sufficient to cause them to interact with membranes differently (Table 5 and Figure 2). In particular, they displayed different exchange dynamics, which provided a means for correlation with antimicrobial activity. LL-23 with a defect on the hydrophobic surface (Figure 7) was unable to effectively penetrate bacterial outer membranes and interacted poorly with outer membrane defective bacteria. However, a substitution of Ser9 of LL-23 with a hydrophobic residue Val, as observed in homologous primate cathelicidins, led to a continuous

dx.doi.org/10.1021/bi2016266 | Biochemistry 2012, 51, 653−664

hydrophobic surface on LL-23V9, allowing a deeper penetration into the bacterial membranes of outer membrane defective bacteria to exert its damaging effects. Our H−D exchange data also indicate that alteration of residues was directly responsible for this enhanced ability and caused a shift of the slowed exchanged residues from the C-terminus of the peptide (Val21 disappeared) to the hot spot (residue 9 remained) (Table 5). In addition, while LL-23 had modest chemokine inducing activity, its variants showed distinct and potent immunomodulatory activities (Figure 1). Thus, a very minor sequence change on the common structural scaffold of LL-23 led to peptides with dramatically different and potent immunomodulatory properties as a consequence of the differences in their dynamic interactions with cells. In conclusion, a single amino acid change on the hydrophobic surface of LL-23 substantially modulated its antimicrobial as well as immune modulating activities. In contrast, a similar modification on LL-37 did not alter its immune modulating activities but reduced its antimicrobial activity only slightly (Figure 1 and Table 1). We propose that the LL-23 family investigated here represents interesting templates for designing distinct and new immune modulating peptides. Because these peptides primarily modulate the human immune system, there is little chance for bacteria to develop resistance. In particular, our observation that LL-23V9 by itself was unable to induce MCP-1 might be of use in designing anti-inflammatory peptides to treat inflammatory diseases such as asthma, rheumatoid arthritis, inflammatory bowel disease, and atherosclerosis.[3,60,61]

AUTHOR INFORMATION

Corresponding Author

*Department of Pathology and Microbiology, University of Nebraska Medical Center, 986495 Nebraska Medical Center, Omaha, NE 68198-6495. Phone: (402) 559-4176. Fax: (402) 559-4077. E-mail: gwang@unmc.edu.

Funding

Research grants from the National Institutes of Health to G.W. and CIHR to R.E.W.H. are gratefully acknowledged. In addition, the Nebraska Research Initiative funding to G.W. allowed for the purchase of a new Bruker Avance III 400 MHz NMR spectrometer and a HPLC system. R.E.W.H. holds a Canada Research Chair.

ACKNOWLEDGMENTS

We thank Dr. Nicole Kruse (Bruker Biospin) for assistance in implementation of the DOSY technique and Dr. Biswajit Mishra (University of Nebraska Medical Center) for HPLC measurements.

ABBREVIATIONS

AMPs, antimicrobial peptides; DPC, dodecylphosphocholine; D8PG, dioctanoylphosphatidylglycerol; ELISA, enzyme-linked immunosorbent assay; HSQC, heteronuclear single-quantum coherence spectroscopy; LDH, lactate dehydrogenase; LPS, lipopolysaccharides; MCP-1, monocyte chemotactic protein-1; MBC, minimal bactericidal concentration; MIC, minimal inhibitory concentration; NMR, nuclear magnetic resonance; NOE, nuclear Overhauser enhancement; PBMC, human peripheral blood mononuclear cells; rmsd, root-mean-square deviation; SD, standard deviation; SDS, sodium dodecyl sulfate; TNF-α, tumor necrosis factor α; TOCSY, total correlated spectroscopy.

REFERENCES

(1) Zasloff, M. (2002) Antimicrobial peptides of multicellular organisms. *Nature 415*, 389−395.

(2) Boman, H. G. (2003) Antibacterial peptides: Basic facts and emerging concepts. *J. Intern. Med. 254*, 197−215.

(3) Easton, D. M., Nijnik, A., Mayer, M. L., and Hancock, R. E. W. (2009) Potential of immunomodulatory host defense peptides as novel anti-infectives. *Trends Biotechnol. 27*, 582−590.

(4) Lehrer, R. I., and Ganz, T. (2002) Defensins of vertebrate animals. *Curr. Opin. Immunol. 14*, 96−102.

(5) Zanetti, M. (2005) The role of cathelicidins in the innate host defenses of mammals. *Curr. Issues Mol. Biol. 7*, 179−196.

(6) Lai, Y., and Gallo, R. L. (2009) AMPed up immunity: How antimicrobial peptides have multiple roles in immune defense. *Trends Immunol. 30*, 131−141.

(7) Wang, Z., and Wang, G. (2004) APD: The antimicrobial peptide database. *Nucleic Acids Res. 32*, D590−D592.

(8) Wang, G., Li, X., and Wang, Z. (2009) APD2: The updated antimicrobial peptide database and its application in peptide design. *Nucleic Acids Res. 37*, D933−D937.

(9) Schroder, J. M., and Harder, J. (2006) Antimicrobial skin peptides and proteins. *Cell. Mol. Life Sci. 63*, 469−486.

(10) Yamasaki, K., and Gallo, R. L. (2008) Antimicrobial peptides in human skin disease. *Eur. J. Dermatol. 18*, 1−11.

(11) Glaser, R. (2011) Research in practice: Antimicrobial peptides of the skin. *JDDG: Journal der Deutschen Dermatologischen Gesellschaft 9*, 678−680.

(12) Marchini, G., Lindow, S., Brismar, H., Stabi, B., Berggren, V., Ulfgren, A.-K., Lonne-Rahm, S., Agerberth, B., and Gudmundsson, G. H. (2002) The newborn infant is protected by an innate antimicrobial barrier: Peptide antibiotics are present in the skin and vernix caseosa. *Br. J. Dermatol. 147*, 1127−1134.

(13) Nizet, V., Ohtake, T., Lauth, X., Trowbridge, J., Rudisill, J., Dorschner, R. A., Pestonjamasp, V., Piraino, J., Huttner, K., and Gallo, R. L. (2001) Innate antimicrobial peptide protects the skin from invasive bacterial infection. *Nature 414*, 454−457.

(14) Lee, P. H., Ohtake, T., Zaiou, M., Murakami, M., Rudisill, J. A., Lin, K. H., and Gallo, R. L. (2005) Expression of an additional cathelicidin antimicrobial peptide protects against bacterial skin infection. *Proc. Natl. Acad. Sci. U.S.A. 102*, 3750−3755.

(15) Yamasaki, K., Schauber, J., Coda, A., Lin, H., Dorschner, R. A., Schechter, N. M., Bonnart, C., Descargues, P., Hovnanian, A., and Gallo, R. L. (2006) Kallikrein-mediated proteolysis regulates the antimicrobial effects of cathelicidins in skin. *FASEB J. 20*, 2068−2080.

(16) Yamasaki, K., Di Nardo, A., Bardan, A., Murakami, M., Ohtake, T., Coda, A., Dorschner, R. A., Bonnart, C., Descargues, P., Hovnanian, A., Norhenn, V. B., and Gallo, R. L. (2007) Increased serine protease activity and cathelicidin promotes skin inflammation in rosacea. *Nat. Med. 13*, 975−980.

(17) Li, Y., Li, X., and Wang, G. (2007) On-resin cleavage of bacterially expressed fusion proteins for purification of active recombinant peptides SK-29, KR-20, LL-29, and LL-23 from human sweat or skin. *Protein Expression Purif. 55*, 395−405.

(18) Wang, G. (2008) Structures of human host defense cathelicidin LL-37 and its smallest antimicrobial peptide KR-12 in lipid micelles. *J. Biol. Chem. 283*, 32637−32643.

(19) Wang, G., Li, Y., and Li, X. (2005) Correlation of three-dimensional structures with the antibacterial activity of a group of peptides designed based on a nontoxic bacterial membrane anchor. *J. Biol. Chem. 280*, 5803−5811.

(20) Dorschner, R. A., Lopez-Garcia, B., Peschel, A., Kraus, D., Morikawa, K., Nizet, V., and Gallo, R. L. (2006) The mammalian ionic environment dictates microbial susceptibility to antimicrobial defense peptides. *FASEB J. 20*, 35−42.

(21) Wiegand, I., Hilpert, K., and Hancock, R. E. W. (2008) Agar and broth dilution methods to determine the minimal inhibitory concentration (MIC) of antimicrobial substances. *Nat. Protoc. 3*, 163−175.

(22) Mookherjee, N., Brown, K. L., Bowdish, D. M. E., Doria, S., Falsafi, R., Hokamp, K., Roche, F. M., Mu, R., Doho, G. H., Pistolic, J., Powers, J., Bryan, J., Brinkman, F. S. L., and Hancock, R. E. W. (2006) Modulation of the TLR-mediated inflammatory response by the endogenous human host defense peptide LL-37. *J. Immunol. 176*, 2455−2464.
(23) Wu, M., and Hancock, R. E. W. (1999) Interaction of the cyclic antimicrobial cationic peptide bactenecin with the outer and cytoplasmic membrane. *J. Biol. Chem. 274*, 29−35.
(24) Keifer, P. A., Peterkofsky, A. P., and Wang, G. (2004) Effects of detergent alkyl chain length and chemical structure on the properties of a micelle-bound bacterial membrane targeting peptide. *Anal. Biochem. 331*, 33−39.
(25) Morris, K. F., and Johnson, C. S. (1992) Diffusion-ordered two-dimensional nuclear magnetic resonance spectroscopy. *J. Am. Chem. Soc. 114*, 3139−3141.
(26) Jeener, J., Meier, B. H., Bachmann, P., and Ernst, R. R. (1979) Investigation of exchange processes by two-dimensional NMR spectroscopy. *J. Chem. Phys. 71*, 4546−4553.
(27) Bax, A., and Davis, D. G. (1985) MLEV-17 based two-dimensional homonuclear magnetization transfer spectroscopy. *J. Magn. Reson. 65*, 355−360.
(28) Rance, M., Sørensen, O. W., Bodenhausen, G., Wagner, G., Enrst, R. R., and Wüthrich, K. (1983) Improved spectral resolution in COSY ^{1}H NMR spectra of proteins via double quantum filtering. *Biochem. Biophys. Res. Commun. 117*, 479−485.
(29) Wang, G. (2006) Structural biology of antimicrobial peptides by NMR spectroscopy. *Curr. Org. Chem. 10*, 569−581.
(30) Kay, L. E., Keifer, P. A., and Saarinen, T. (1992) Pure absorption gradient enhanced heteronuclear single quantum correlation spectroscopy with improved sensitivity. *J. Am. Chem. Soc. 114*, 10663−10665.
(31) Bax, A., and Grzesiek, S. (1993) Methodological advances in protein NMR. *Acc. Chem. Res. 26*, 131−138.
(32) Markley, J. L., Bax, A., Arata, Y., Hilbers, C. W., Kaptein, R., Sykes, B. D., Wright, P. E., and Wüthrich, K. (1998) Recommendations for the presentation of NMR structures of proteins and nucleic acids. IUPAC-IUBMB-IUPAB Inter-Union Task Group on the Standardization of Data Bases of Protein and Nucleic Acid Structures Determined by NMR Spectroscopy. *J. Biomol. NMR 12*, 1−23.
(33) Delaglio, F., Grzesiek, S., Vuister, G. W., Zhu, G., Pfeifer, J., and Bax, A. (1995) NMRPipe: A multidimensional spectral processing system based on UNIX pipes. *J. Biomol. NMR 6*, 277−293.
(34) Garrett, D. S., Powers, R., Gronenborn, A. M., and Clore, G. M. (1991) A common sense approach to peak picking two-, three- and four-dimensional spectra using automatic computer analysis of contour diagrams. *J. Magn. Reson. 95*, 214−220.
(35) Wüthrich, K. (1986) *NMR of Proteins and Nucleic Acids*, Wiley, New York.
(36) Cornilescu, G., Delaglio, F., and Bax, A. (1999) Protein backbone angle restraints from searching a database for chemical shift and sequence homology. *J. Biomol. NMR 13*, 289−302.
(37) Schwieters, C. D., Kuszewski, J., Tjandra, N., and Clore, G. M. (2003) The Xplor-NIH NMR molecular structure determination package. *J. Magn. Reson. 160*, 65−73.
(38) Koradi, R., Billeter, M., and Wüthrich, K. (1996) MOLMOL: A program for display and analysis of macromolecular structures. *J. Mol. Graphics 14*, 51−55.
(39) Laskowski, R. A., Rullmannn, J. A., MacArthur, M. W., Kaptein, R., and Thornton, J. M. (1996) AQUA and PROCHECK-NMR: Programs for checking the quality of protein structures solved by NMR. *J. Biomol. NMR 8*, 477−486.
(40) Scott, M. G., Dullaghan, E., Mookherjee, N., Glavas, N., Waldbrook, M., Thompson, A., Wang, A., Lee, K., Doria, S., Hamill, P., Yu, J., Li, Y., Donini, O., Guarna, M. M., Finlay, B. B., North, J. R., and Hancock, R. E. W. (2007) An anti-infective peptide that selectively modulates the innate immune response. *Nat. Biotechnol. 25*, 465−472.
(41) Nijnik, A., Madera, L., Ma, S., Waldbrook, M., Elliott, M. R., Easton, D. M., Mayer, M. L., Mullaly, S. C., Kindrachuk, J., Jenssen, H., and Hancock, R. E. W. (2010) Synthetic cationic peptide IDR-1002 provides protection against bacterial infections through chemokine induction and enhanced leukocyte recruitment. *J. Immunol. 184*, 2539−2550.
(42) Bowdish, D. M., Davidson, D. J., Speert, D. P., and Hancock, R. E. W. (2004) The human cationic peptide LL-37 induces activation of the extracellular signal-regulated kinase and p38 kinase pathways in primary human monocytes. *J. Immunol. 172*, 3758−3765.
(43) Wang, G., Keifer, P. A., and Peterkofsky, A. (2003) Solution structure of the N-terminal amphitropic domain of *Escherichia coli* glucose-specific enzyme IIA in membrane-mimetic micelles. *Protein Sci. 12*, 1087−1096.
(44) Wang, G., Keifer, P. A., and Peterkofsky, A. (2004) Short-chain diacyl phosphatidylglycerols: Which one to choose for NMR structural determination of a membrane-associated peptide from *Escherichia coli*? *Spectroscopy 18*, 257−264.
(45) Farrow, N. A., Muhandiram, R., Singer, A. U., Pascal, S. M., Kay, C. M., Gish, G., Shoelson, S. E., Pawson, T., Foeman-Kay, J. D., and Kay, L. E. (1994) Backbone dynamics of a free and phosphopeptide-complexed Src homolog 2 domain studied by ^{15}N NMR relaxation. *Biochemistry 33*, 5984−6003.
(46) Wang, G. (2008) NMR studies of a model antimicrobial peptide in the micelles of SDS, dodecylphosphocholine, or dioctanoylphosphatidylglycerol. *Open Magn. Reson. J. 1*, 9−15.
(47) Wang, G., Treleaven, D., and Cushley, R. J. (1996) Conformation of human serum apolipoprotein A-I(166−185) in the presence of sodium dodecyl sulfate or dodecylphosphocholine by ^{1}H-NMR and CD. Evidence for specific peptide-SDS interactions. *Biochim. Biophys. Acta 1301*, 174−184.
(48) Porcelli, F., Verardi, R., Shi, L., Henzler-Wilderman, K. A., Ramamoorthy, A., and Veglia, G. (2008) NMR structure of the cathelicidin-derived human antimicrobial peptide LL-37 in dodecylphosphocholine micelles. *Biochemistry 47*, 5565−5572.
(49) Li, X., Li, Y., Han, H., Miller, D. W., and Wang, G. (2006) Solution structures of human LL-37 fragments and NMR-based identification of a minimal membrane-targeting antimicrobial and anticancer region. *J. Am. Chem. Soc. 128*, 5776−5785.
(50) Zelezetsky, I., Pontillo, A., Puzzi, L., Antcheva, N., Segat, L., Pacor, S., Crovella, S., and Tossi, A. (2006) Evolution of the primate cathelicidin. Correlation between structural variations and antimicrobial activity. *J. Biol. Chem. 281*, 19861−19871.
(51) Lau, Y. E., Rozek, A., Scott, M. G., Goosney, D. L., Davidson, D. J., and Hancock, R. E. W. (2005) Interaction and cellular localization of the human host defense peptide LL-37 with lung epithelial cells. *Infect. Immun. 73*, 583−591.
(52) Mookherjee, N., Lippert, D. N. D., Hamill, P., Falsafi, R., Nijnik, A., Kindrachuk, J., Pistolic, J., Gardy, J., Miri, P., Naseer, M., Foster, L. J., and Hancock, R. E. W. (2009) Intracellular receptor for human host defense peptide LL-37 in monocytes. *J. Immunol. 183*, 2688−2696.
(53) Braff, M. H., Hawkins, M. A., Di Nardo, A., Lopez-Garcia, B., Howell, M. D., Wong, C., Lin, K., Streib, J. E., Dorschner, R., Leung, D. Y., and Gallo, R. L. (2005) Structure-function relationships among human cathelicidin peptides: Dissociation of antimicrobial properties from host immunostimulatory activities. *J. Immunol. 174*, 4271−4278.
(54) Mookherjee, N., Wilson, H. L., Doria, S., Popowych, Y., Falsafi, R., Yu, J., Li, Y., Veatch, S., Roche, F. M., Brown, K. L., Brinkman, F. S., Hokamp, K., Potter, A., Babiuk, L., Griebel, P. J., and Hancock, R. E. W. (2006) Bovine and human cathelicidin cationic host defense peptides similarly suppress transcriptional responses to bacterial lipopolysaccharide. *J. Leukocyte Biol. 80*, 1563−1774.
(55) Rosenfeld, Y., Papo, N., and Shai, Y. (2006) Endotoxin (lipopolysaccharide) neutralization by innate immunity host-defense peptides. *J. Biol. Chem. 281*, 1636−1643.
(56) Turner, J., Cho, Y., Dinh, N.-N., Waring, A. J., and Lehrer, R. I. (1998) Activities of LL-37, a cathelin-associated antimicrobial peptides of human neutrophils. *Antimicrob. Agents Chemother. 42*, 2206−2214.
(57) Nagaoka, I., Hirota, S., Niyonsaba, F., Hirata, M., Adachi, Y., Tamura, H., Tanaka, S., and Heumann, D. (2002) Augmentation of the lipopolysaccharide-neutralizing activities of human cathelicidin

CAP18/LL-37-derived antimicrobal peptides by replacement with hydrophbic and cationic amino acid residues. *Clin. Diagn. Lab. Immunol. 9*, 972−982.
(58) Wang, G., Epand, R. F., Mishra, B., Lushnikova, T., Thomas, V. C., Bayles, K. W., and Epand, R. M. (2011) Decoding the functional roles of cationic side chains of the major antimicrobial region of human cathelicidin LL-37. *Antimicrob. Agents Chemother.*, doi: 10.1128/AAC.05637-11.
(59) Wu, W. K. K., Wang, G., Coffelt, S. B., Betancourt, A. M., Lee, C. W., Yu, J., Sung, J. J. Y., and Cho, C. H. (2010) Emerging roles of the host defense peptide LL-37 in human cancer and its potential therapeutic applications. *Int. J. Cancer 127*, 1741−1747.
(60) Wang, G. (2010) *Antimicrobial Peptides: Discovery, Design and Novel Therapeutic Strategies*, CABI, Wallingford, England.
(61) Edfeldt, K., Agerberth, B., Rottenberg, M. E., Gudmundsson, G. H., Wang, X. B., Mandal, K., Xu, Q., and Yan, Z. Q. (2006) *Arterioscler. Thromb. Vasc. Biol. 26*, 1551−1557.
(62) Staubiz, P., Neumann, H., Schneider, T., Wiedemann, I., and Peschel, A. (2004) MprF-mediated biosynthesis of lysylphosphatidylglycerol, an important determinant in staphylococcal defensin resistance. *FEMS Microbiol. Lett. 231*, 67−71.
(63) Van de Ven, F. J. M. (1995) *Multidimensional NMR in Liquids*, Wiley-VCH, New York.